Journal of Power Sources 196 (2011) 8675–8682

Contents lists available at ScienceDirect

Journal of Power Sources

journal homepage: www.elsevier.com/locate/jpowsour

Influence of particle size on the self-discharge behavior of graphite electrodes in lithium-ion batteries

Takashi Utsunomiya[a,b], Osamu Hatozaki[b], Nobuko Yoshimoto[a], Minato Egashira[a], Masayuki Morita[a,*]

[a] Department of Applied Chemistry, Graduate School of Science and Engineering, Yamaguchi University, 2-16-1, Tokiwadai, Ube 755-8611, Japan
[b] Subaru Technical Research Center, Fuji Heavy Industries Ltd., 9-6-3, Ohsawa, Mitaka 181-8577, Japan

ARTICLE INFO

Article history:
Received 24 May 2011
Received in revised form 20 June 2011
Accepted 21 June 2011
Available online 28 June 2011

Keywords:
Self-discharge
Graphite
Particle size
Lithium-ion battery
SEI formation

ABSTRACT

Self-discharge characteristics of synthetic graphite electrodes with different particle sizes have been investigated by electrochemical and analytical methods. Variations of open-circuit potential (OCP), residual capacity and electrochemical impedance responses were monitored during or after the storage at different temperatures. The rate of self-discharge depended on the particle size, or the specific surface area, of the graphite sample. The temperature dependence of the self-discharge rate revealed that the activation energy for the process does not depend on the particle size of the graphite electrode. The ac impedance responses suggest that the self-discharge processes consist of the loss of the Li species in the graphite and SEI (Solid-Electrolyte-Interphase) formation at the graphite surface. The latter SEI formation process was found to be dependent on the surface site, edge or basal planes, from the results of surface observation and elemental analyses.

1. Introduction

Losing charge capacity of a battery after the storage for a certain period is generally called self-discharge. It may affect not only the battery performance itself but also the safety issue of the power system. If the rates of self-discharge at positive and negative electrodes are significantly different, the balance in the electrode potential would shift toward the electrode keeping higher state-of-charge (SOC), which would result in the over-charge of the electrode in problem. Thus, it becomes much more important to have sufficient knowledge on the self-discharge processes when developing such larger-sizes of lithium-ion batteries (LIBs) as in electric vehicle (EV) uses.

Possible causes for self-discharge of LIB systems are considered to be undesirable chemical processes occurring at positive and negative electrodes. Some research groups have reported theoretical and experimental results on the self-discharge processes of LIBs and the electrodes therein [1,2]. Among them, relation between the self-discharge of carbon-based negative electrode and the interfacial reaction forming so-called Solid-Electrolyte-Interphase (SEI) has been analyzed by Yazami and co-workers [3–5]. The SEI formation processes at carbon electrodes themselves have also been investigated from the viewpoints of irreversible capacity loss in the initial cycles [6–8] and the cycle deterioration of the discharge capacity of carbon negative electrodes [9,10]. In brief, the capacity losses of the lithiated carbon electrodes during the long-term storage in organic electrolyte solutions associate with the formation and growth of the surface film, or SEI. On the other hand, Kinoshita and co-workers [11] pointed out the importance of the bulk reaction of the organic electrolyte in the self-discharge behavior of LIB. The thermal stability of SEI has also been investigated from the viewpoint of the safety issue of the cell system [12,13]. Although a mathematical model has been presented to simulate the capacity loss by self-discharge in commercial LIB [14], there still remains unclear among the relation between the self-discharge behavior and the surface processes at carbonaceous electrodes.

We have also examined the self-discharge processes at some kinds of carbon-based negative electrodes in organic electrolyte systems, and demonstrated that monitoring open-circuit potential (OCP) during the storage at constant temperature is useful to discuss the extent of the self-discharge of lithiated carbon electrodes [15,16]. The effectiveness of the OCP monitoring to detect the extent of self-discharge has already been proved for lithiated graphite electrode by Wang et al. [17]. In the present work, we have investigated the influences of the particle size on the self-discharge behavior of synthetic graphite electrodes. That is, variations in OCP and equivalent series resistance (ESR) of the lithiated graphite were recorded with the storage time as a function of the temperature.

It is of practical importance to understand the influences of the particle size on the self-discharge rate because LIBs with high-rate capability tends to use smaller particle sizes of the electrode active materials. Thus, in this work, the self-discharge rates for dif-

* Corresponding author. Tel.: +81 836 85 9211; fax: +81 836 85 9201.
E-mail address: morita@yamaguchi-u.ac.jp (M. Morita).

0378-7753/$ – see front matter © 2011 Elsevier B.V. All rights reserved.
doi:10.1016/j.jpowsour.2011.06.070

Table 1
Characteristics of the graphite samples examined in the present work.

Graphite sample	XRD	Particle size distribution (μm)			Specific surface area ($m^2\ g^{-1}$)
	$d(002)$ (10^{-1} nm)	D10	D50	D90	
KS-4	3.366	2.7	4.8	7.6	21.7
KS-10	3.368	4.2	6.9	10.9	12.1
KS-25	3.368	5.4	8.9	14.2	10.4

ferent particle sizes were estimated from the residual discharge capacity after the storage, and their temperature dependences were discussed from the viewpoint of the changes in the process at the electrode/electrolyte interface. The surface analyses were also conducted for self-discharged graphite electrodes by means of scanning transmission electron microscope (STEM) combined with energy dispersive X-ray spectroscopy (EDX).

2. Experimental

Three kinds of powdered synthetic flake graphite with different average particle sizes (KS4, KS10, and KS25, from Timical) were used as the test electrode. The specific surface area and XRD characteristics of the materials are listed in Table 1. The test electrodes were prepared by the same procedure as that described previously [16]. Those were composed of 88% (in mass) of the active material, 5% of carbon black, 3% of carboxymethylcellulose (CMC) as a dispersant, and 4% of styrene-butadiene rubber (SBR) as a binder. Slurry of the active material with the dispersant and the binder was made in distillated water, which was coated on a copper-foil current collector. The thickness of the active material was controlled to ca. 25 μm.

The test cell was a laminated three-electrode cell [16] consisting of the graphite negative electrode as the test electrode, a chip of lithium (Li) foil as the reference and a large surface area Li foil as the counter electrodes. The geometric working area of the test electrode was 4.0 cm^2 (20 mm × 20 mm). The electrolyte solution was 1.2 mol dm^{-3} (M) $LiPF_6$ dissolved in mixed solvent of ethylene carbonate (EC) and diethyl carbonate (DEC) with 1:3 volume ratio (1.2 M $LiPF_6$/EC3DEC). The water content in the resulting electrolyte solution was lower than 20 ppm.

The charge and discharge cycling was carried out under a constant-current condition coupled with constant-potential (CC–CP) charging, where the term "charging" means the cathodic lithiation of the negative electrodes and the "discharging" the anodic de-lithiation in this paper [15,16]. Constant current of 1 mA, which is equivalent to $C/10$ rate, was applied for charging and discharging of the negative electrode. The cut-off potential and time for charging were 30 mV vs. Li/Li^+ and 10 h, respectively.

Variations in OCP and ESR were monitored for ca. 24 h after the first charging in a thermostatically controlled oven. The storage temperature was ranged from −20 to 60 °C. After the storage for each period, the residual capacity of the graphite electrode was determined by constant current discharging with $C/10$ rate. An ac impedance method was applied to analyze the interfacial processes during the storage of the charged (lithiated) electrodes. The frequency was scanned from 100 kHz to 10 mHz with 10 mV_{p-p} ac amplitude under the OCP conditions at room temperature. All electrochemical measurements were carried out under a dry argon atmosphere.

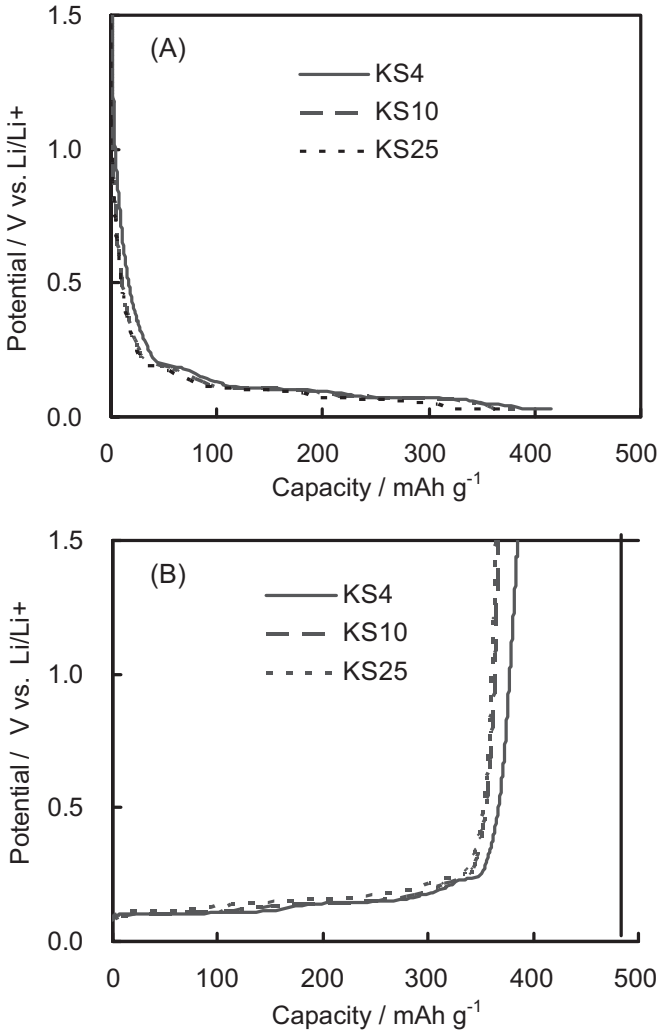

Fig. 1. Charge and discharge curves of the synthetic flake graphite electrodes in 1.2 mol dm^{-3}. $LiPF_6$/EC + DEC (1:3) at 25 °C; electrode: (A) KS4, (B) KS10, and (C) KS25.

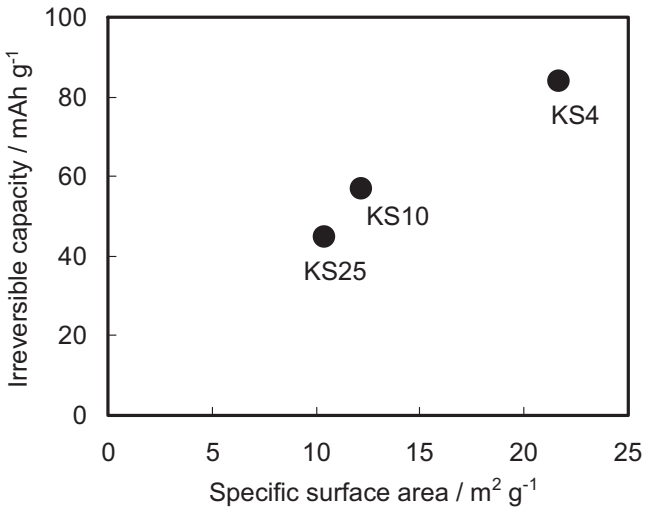

Fig. 2. Correlation between the irreversible capacity in the first cycle and the specific surface area of the graphite samples.

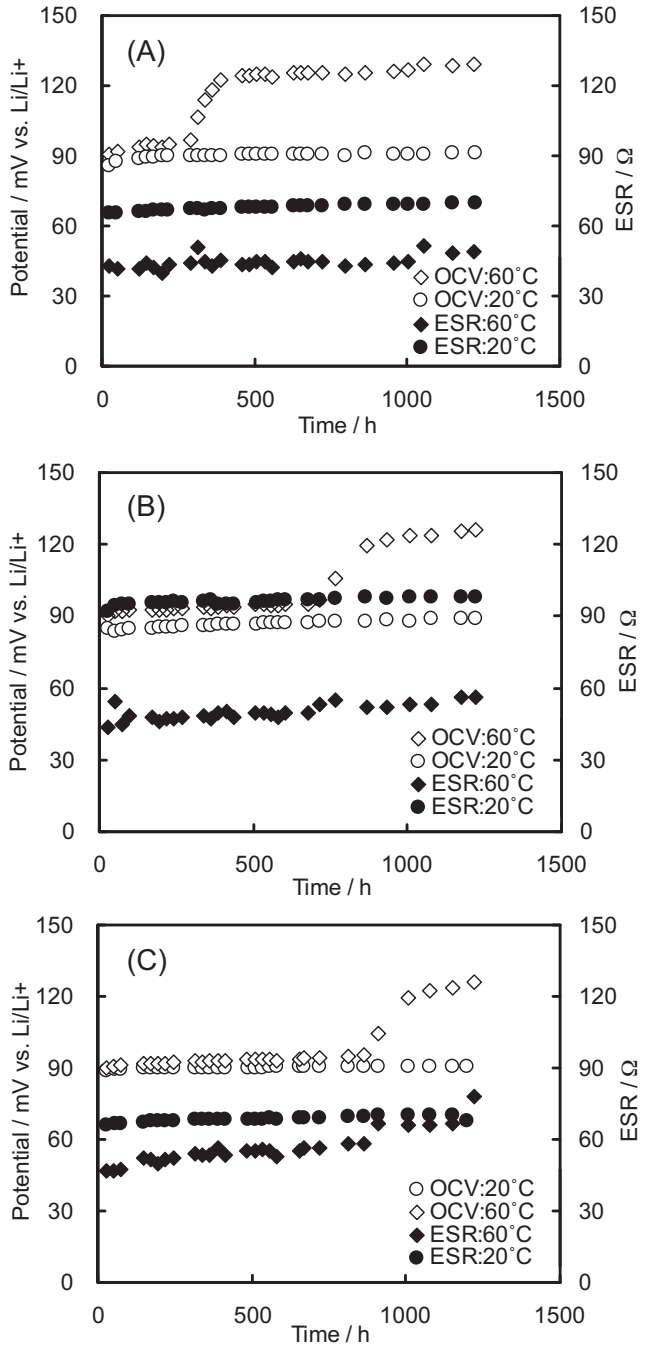

Fig. 3. Variations in OCP and ESR for synthetic flake graphite electrodes in 1.2 mol dm^{-3} $LiPF_6$/EC + DEC (1:3) at 20 °C (circles) and 60 °C (squares). Electrode: (A) KS4, (B) KS10, and (C) KS25; open symbols: OCP; closed symbols: ESR.

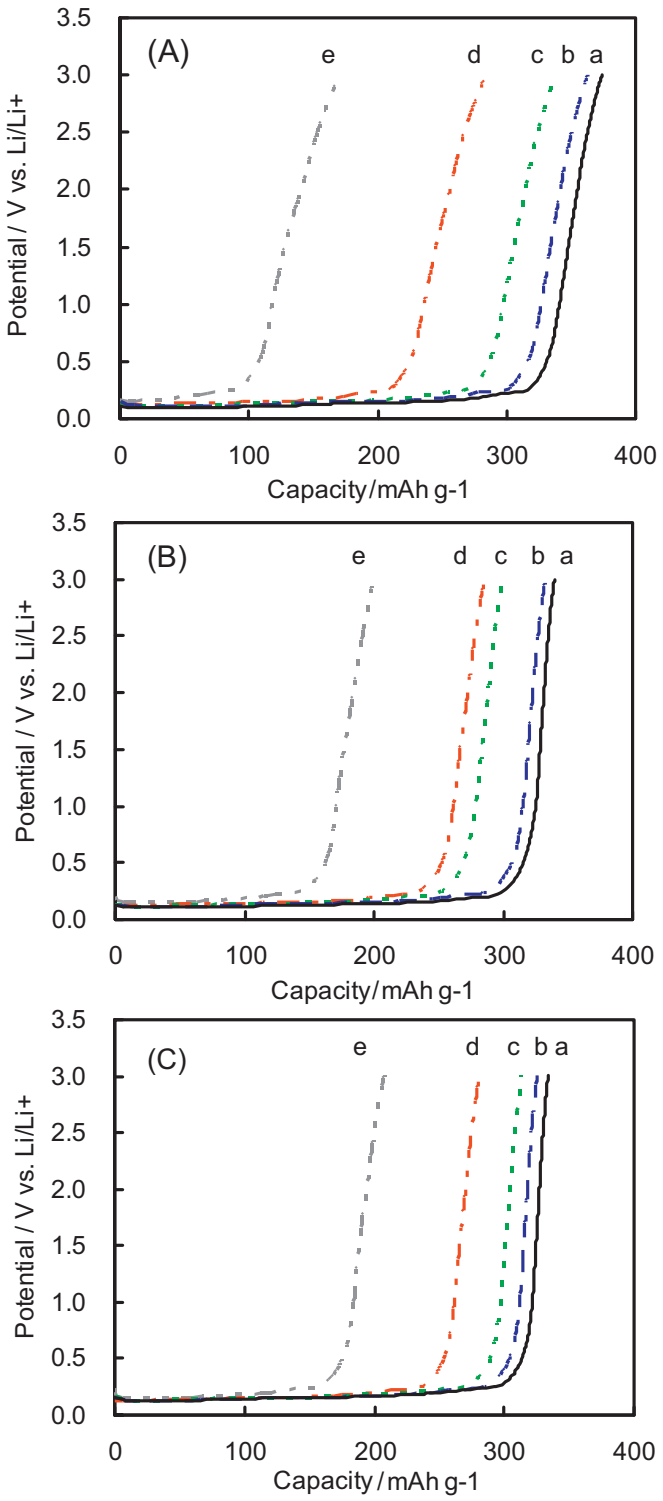

Fig. 4. Variations in the discharge curves of the synthetic flake graphite electrodes after the OCP measurements for 51 days in 1.2 mol dm^{-3} $LiPF_6$/EC + DEC (1:3) at different temperature. Electrode: (A) KS4, (B) KS10, and (C) KS25; temperature: −20 °C (a), 0 °C (b), 20 °C (c), 40 °C (d), and 60 °C (e).

The surface observation experiments were carried out for the graphite particles after the storage at different temperatures. The self-discharged graphite electrodes were rinsed carefully with DEC solvent to remove the electrolytic salt and dried in an argon atmosphere. The test electrodes were moved from the glove box to a focused ion beam (FIB: Hitach, FB2000A) chamber attached to an STEM equipment (JEOL, JEM2100F), using a transfer vessel to avoid the sample exposed to an atmosphere. A test piece was cut down from the surface (electrolyte) side of the electrode using FIB. The surface morphology and the element distribution were observed by STEM coupled with EDX (JEOL, JED2300T).

3. Results and discussion

Table 1 summarizes the results of instrumental analyses for carbon samples examined in this work. All of carbon materials were found to be graphite with high crystalline by XRD patterns and Raman spectra. No significant differences were observed in $d(0\,0\,2)$

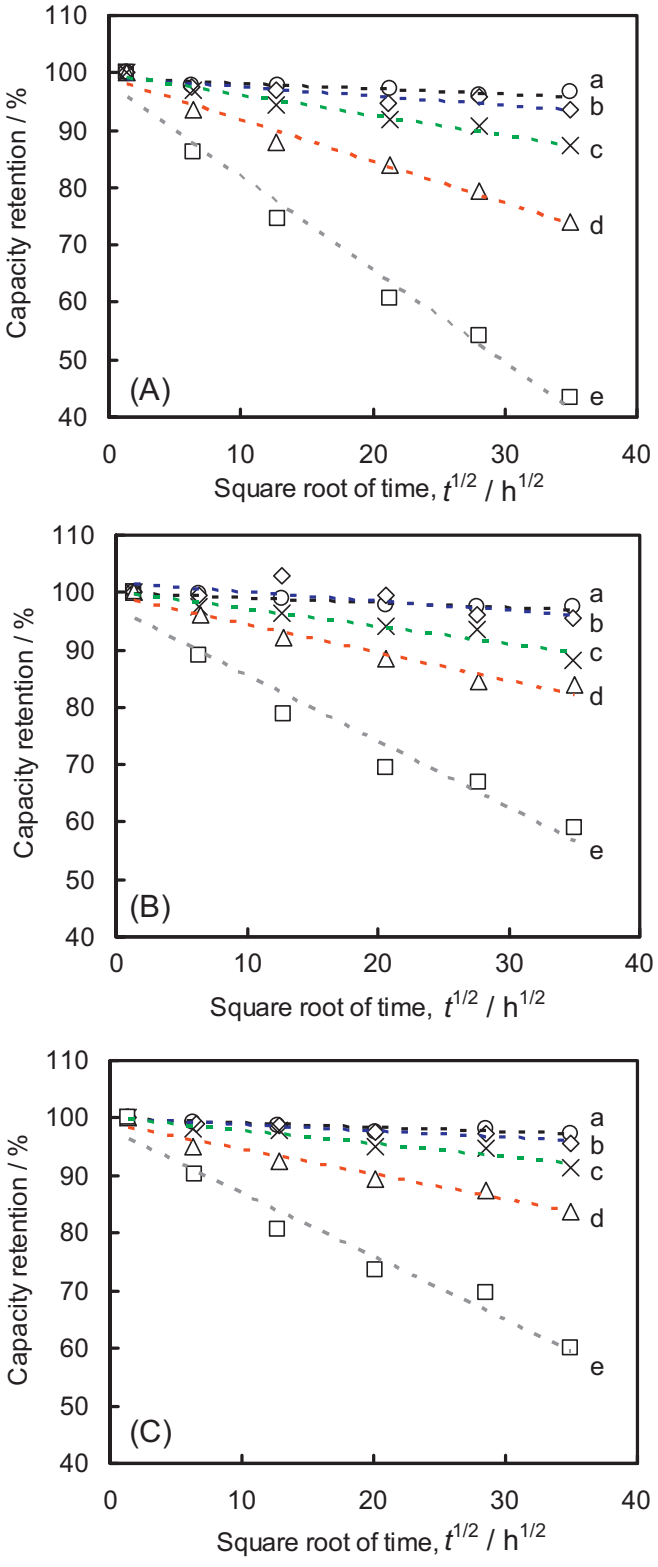

Fig. 5. Variations in the capacity retention with the square root of storage time in 1.2 mol dm^{-3} $LiPF_6$/EC + DEC (1:3). Electrode: (A) KS4, (B) KS10, and (C) KS25; temperature: −20 °C (a), 0 °C (b), 20 °C (c), 40 °C (d), and 60 °C (e).

values of XRD among the samples. Also the relative intensity of the D/G bands in Raman spectra was almost constant (2.3–4.1) throughout the samples. The specific surface area determined by a BET method tends to decrease with the increase in the particle size distribution, KS4 > KS10 > KS25.

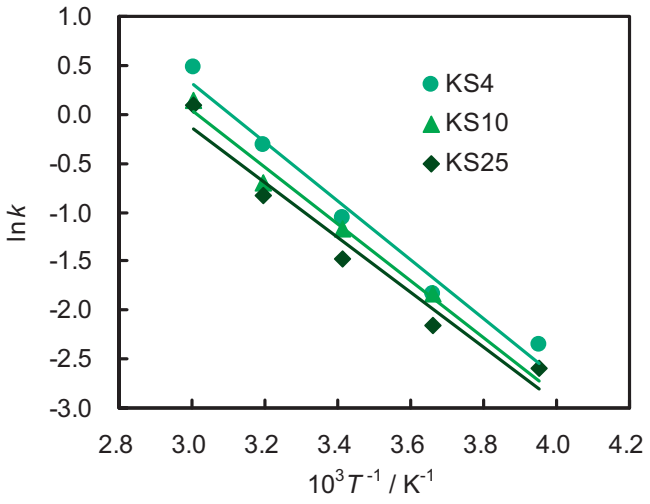

Fig. 6. Arrhenius plots of the relative rate constant (k) for self-discharge obtained from Fig. 5. Electrode: (●) KS4, (▲) KS10, (♦) KS25.

In Fig. 1, charge and discharge curves at 1/10 rate are shown for each graphite sample in its second cycle. For every electrode, potential plateaus corresponding to the stage structures of graphite-intercalation compounds (GIC) were observed on the curves. There was no significant difference in the discharge capacity among the samples under a current rate of 1/10*C*, except for the steep potential increase at the end of discharge, revealing the discharge capacity of about 370 mAh g^{-1}, which is theoretically expected for ideal graphite. However, so-called irreversible capacity (difference between the first charge and discharge capacities) depended on the sample. Fig. 2 shows the relation between the irreversible capacity of the first cycle and the specific surface area for the samples examined. The irreversible capacity tends to increase with the increase in the specific surface area. This is probably related with the extent of such surface processes as SEI formation during the first charge. As the irreversible surface process depends on the active surface area, the irreversible capacity generally increases with the specific surface area of the graphite sample.

Fig. 3 shows the variations in open-circuit potential (OCP) and equivalent series resistance (ESR) of the graphite electrodes after the second charge in $LiPF_6$/EC3DEC solution at different temperatures. Variations in OCP with the storage time corresponded to

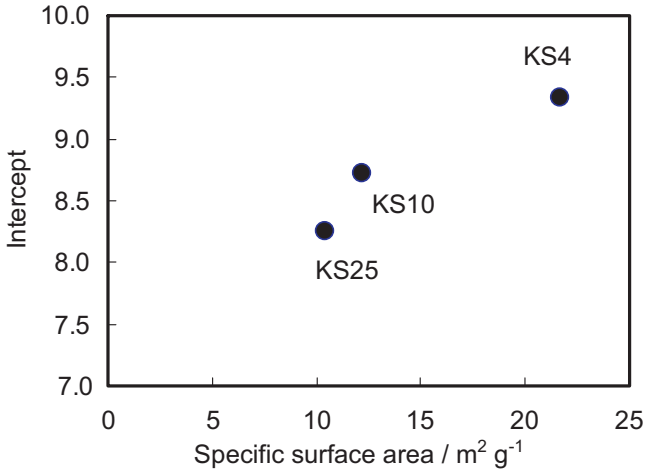

Fig. 7. Correlation between the pre-exponential factor of the Arrhenius plot and the specific surface area of the graphite samples.

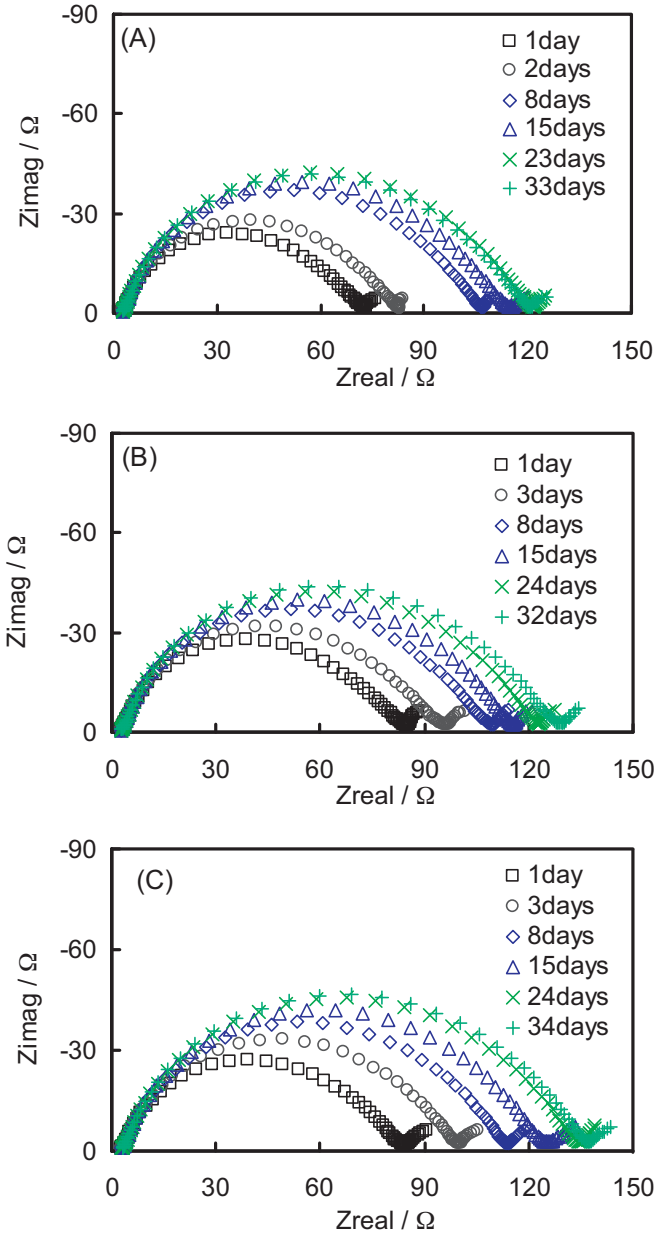

Fig. 8. Variations in the ac impedance after OCP measurements for the synthetic flake graphite in 1.2 M $LiPF_6$/EC + DEC (1:3) at 20 °C.

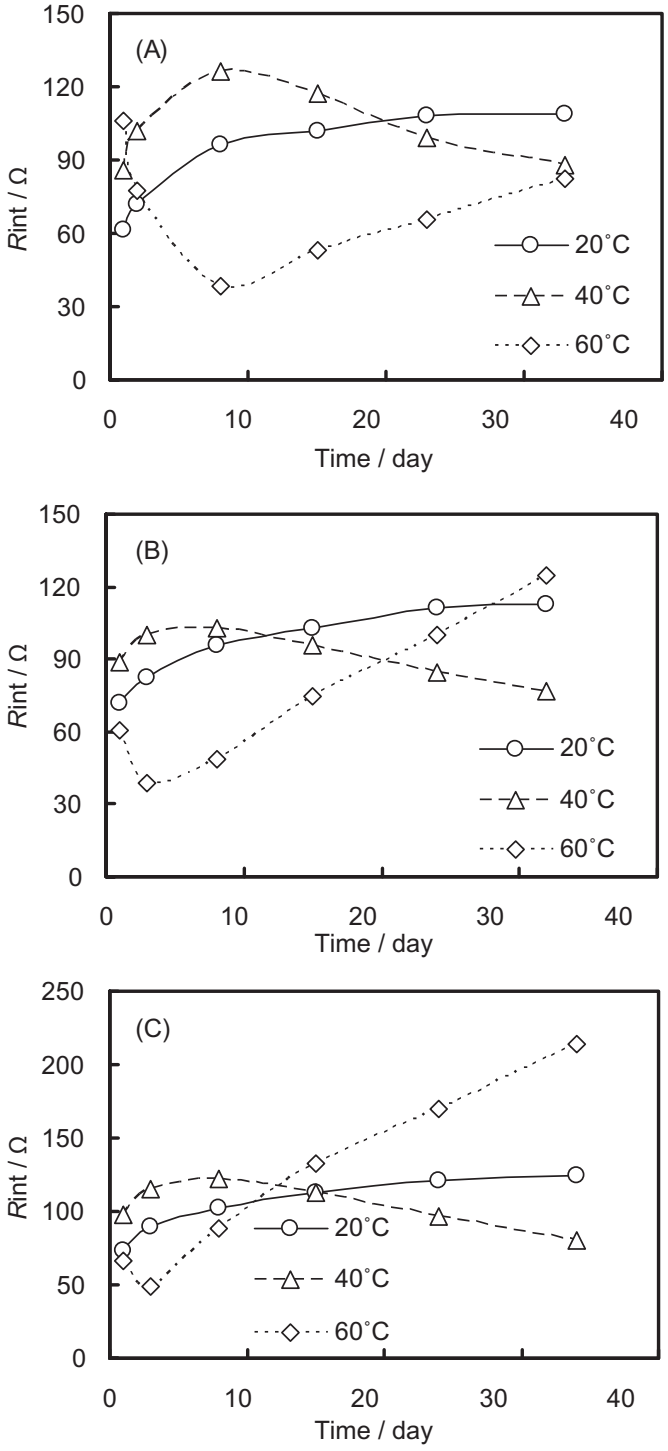

Fig. 9. Variations in the interface resistance (R_{int}) after OCP measurements for the synthetic flake graphite in 1.2 M $LiPF_6$/EC + DEC (1:3).

stepwise changes in the stage structures of Li-GICs. That is, the potential plateau at about 90 mV vs. Li/Li^+ shows that the system keeps in equilibrium between the first stage compound, LiC_6, and its lower stage Li-GIC, whose results are well consistent with previous observations [15,17]. The potential increases from ca. 90 mV to ca. 120 mV during the storage at 60 °C indicate that further changes in the stage structure proceeds with loosing Li species in GIC by self-discharging processes [15]. The time at this steep increase in OCP depended on the sample. It tended to be faster for the sample with smaller particle size. The temperature dependence of OCP value itself in the equilibrium was rather small.

The ESR values of the electrode showed a tendency that the storage at higher temperature gives lower ESR. Its variation with the storage time was rather small, because the major component of ESR observed here was bulk resistance of the electrolyte. However, small stepwise increases were observed for the electrodes stored at 60 °C, whose timing was apparently consistent with the time on the steep increase in the OCP changes.

In Fig. 4, discharge curves after the OCP measurements for 51 days are shown as a function of the storage temperature. The discharge capacity generally decreased with the increase in the temperature. The capacity loss was very small at the −20 °C storage (curves a) for every electrode. With increasing temperature, however, the discharge capacity gradually decreased, and its particle size dependence became clear. These results indicate that the self-

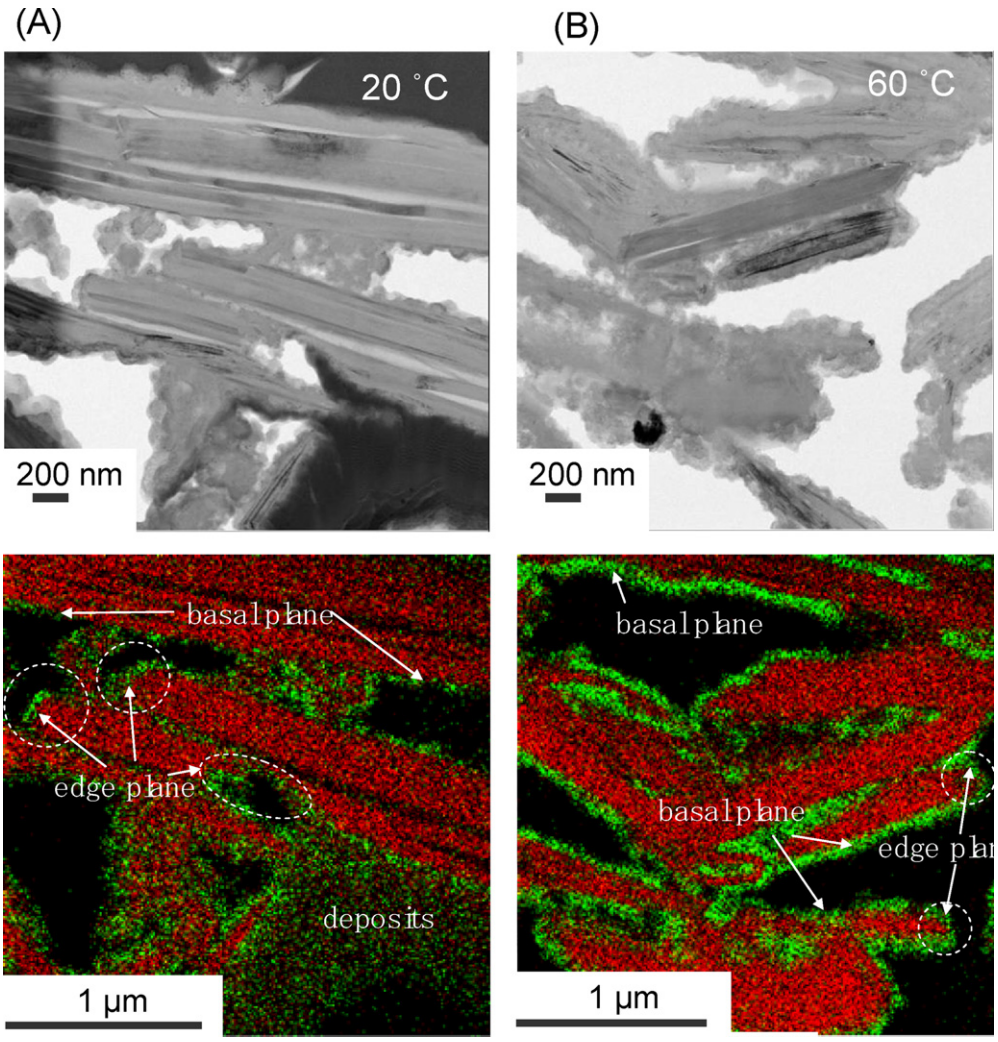

Fig. 10. STEM and EDX images of the synthetic flake graphite (KS4) after the storage for 51 days at 20 °C (A) and 60 °C (B).

discharge rate increases with the storage temperature and depends on the particle size of the graphite sample.

We can define a parameter, capacity retention, as a measure of the extent of self-discharge, using the percent of discharge capacity after the storage to the initial capacity. In Fig. 5, the capacity retention is plotted against square root of the storage time, $t^{1/2}$, for each electrode in different temperatures [15,16]. Almost linear relation between the capacity retention and $t^{1/2}$ was observed for each electrode in every temperature condition. These results suggest that the capacity losing process is controlled by a certain diffusion process. Similar observation was already reported on the self-discharge behavior of lithiated hard carbon [15]. These experimental results are well consistent with a mathematically simulated model assuming certain surface processes associated with the electrolyte reduction consuming Li species in the electrode [14]. The slope of the linear plot for the capacity retention vs. $t^{1/2}$ can be regarded as an apparent rate constant of the self-discharge of lithiated graphite [16].

In Fig. 6, Arrhenius plots of the apparent rate constant for self-discharging, $\ln k$ vs. $1/T$, are shown for the electrodes with different particle sizes. The linear relation of the plots suggests that the capacity losing process is controlled by the same process over the whole temperature range, from −20 to +60 °C. The slope of the Arrhenius plot gives apparent activation energy for the process in question. Almost the same values of ca. 20 kJ mol^{-1} were obtained for the electrodes with different particle sizes. The difference in the self-discharge rate among the electrodes, KS4 > KS10 > KS25, is caused by the difference in the intercept of the Arrhenius plot, or pre-exponential term (frequency factor). In Fig. 7, the relative value of the intercept is plotted against the specific surface area of the graphite particle. Higher specific surface area of the graphite gives higher value of the pre-exponential term, but almost the same activation energy. This result leads to an important conclusion that the mechanism of the self discharge itself does not change with the particle size or specific surface area, but its rate depends much on the active surface area of the graphite. Further, the profile shown in Fig. 7 is quite similar to that in Fig. 2, where the relation between the irreversible capacity and the specific surface area of the material is shown. This also suggests that both of the causes in the capacity loss during the storage and the irreversible capacity at the first cycle have common process that is strongly dependent on the specific surface area of the graphite powder.

Fig. 8 shows the time-course of the ac impedance measured for lithiated graphite electrodes during the storage at 20 °C. For every electrode the Nyquist (complex-plane) plot of the impedance has one semicircle in the high frequency region and a small arc in the lower frequency region. The size of the semicircle, indicating the interface impedance of the electrode, generally increased with the storage time. On the other hand, the bulk resistance, R_{bulk}, which

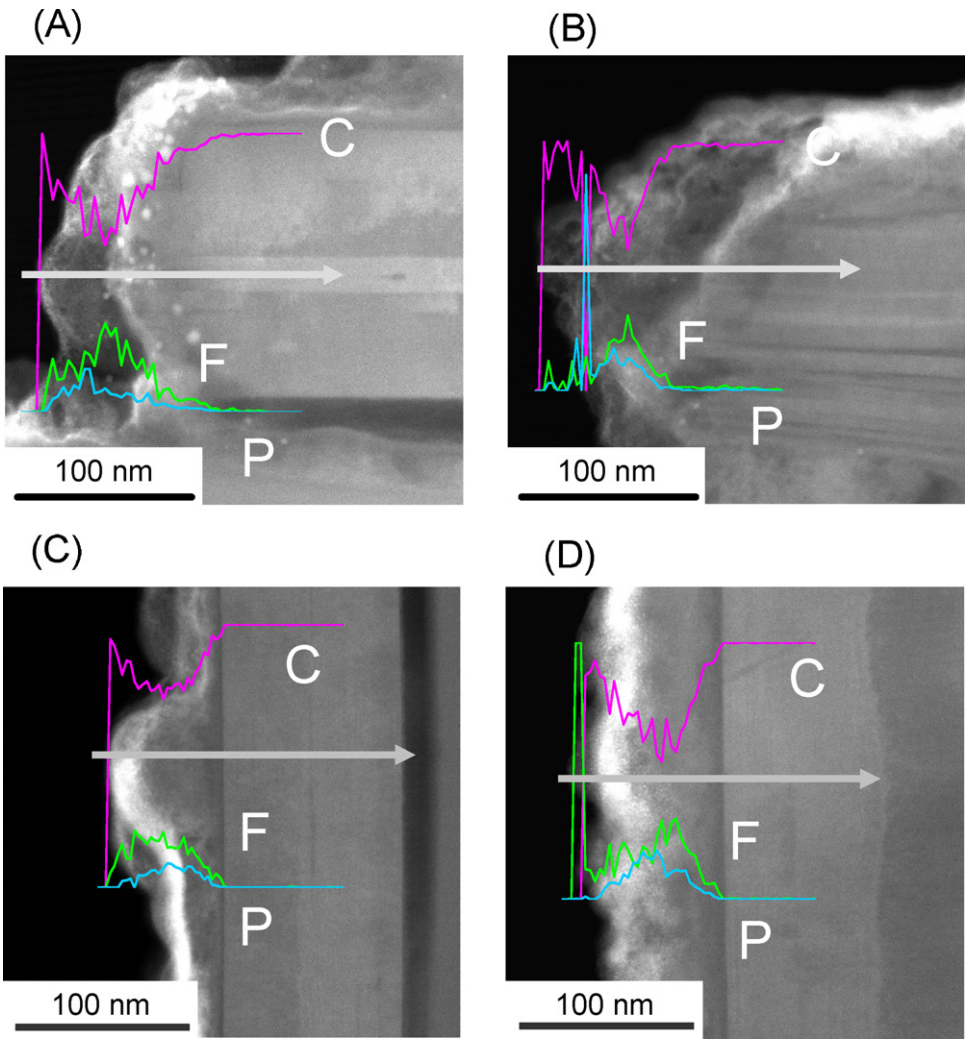

Fig. 11. STEM image and elemental analyses at the edge plane (A, B) and the basal plane (C, D) of synthetic flake graphite (KS4) after the storage for 51 days at 20 °C (A, C) and 60 °C (B, D).

was determined from the intersection of the semicircle with the Z_{real} axis at higher frequency region, did not change significantly during the storage, as discussed previously. Thus, we can assume that the processes influencing the interface impedance will be strongly associated with the capacity loss of the graphite electrode during the storage.

The resistance component of the impedance in the higher frequency region, defined as interface resistance R_{int}, is plotted in Fig. 9, as a function of the storage time for different electrodes at different temperatures. In general, as R_{int} is partly conjugated with the charge-transfer resistance, it will decrease with decreasing the state-of-charge (SOC) of the graphite electrode [6,16]. However, the main reason of increasing R_{int} with the storage time is considered to be the growth of SEI on the graphite surface. For every electrode, variations in R_{int} with time were rather small at lower temperatures, as shown in the data at 20 °C, in which monotonous increases in R_{int} were observed. However, for the storage at 40 °C, the variation of R_{int} gave maxima at around 8 days. For the storage at 60 °C, the R_{int} value decreased once at the initial period of the storage, and then increased with the storage time. Similar results have commonly observed for other carbon materials [16]. We have already given a following scheme to explain such complex behavior in R_{int}. At lower temperature, the self-discharge reaction to grow surface SEI layer is rather low, and then the interface resistance gradually increases but does not show significant change with time. On the other hand, during the storage at higher temperature, e.g. at 60 °C, a higher rate of film forming reaction causes the significant increase in the interface resistance, except for the initial period of the storage where the charge-transfer resistance decreases with the initial decrease in the SOC caused by the loss of Li species in the charged electrode. In a moderate temperature range, e.g. at 40 °C, the growth of the SEI layer increases the interface resistance, but the decrease in SOC caused by the self-discharge lowers the charge-transfer resistance. Competition or balance of these two contributions would result in such variations in R_{int} as shown in Fig. 9, where maximum values are observed at 4–8 days of the storage time.

Results of STEM (scanning transmission electron micrograph) and EDX (energy dispersive X-ray spectroscopy) analyses of the graphite surface (KS4) after the storage at different temperatures are shown in Figs. 10 and 11. The distributions of C and F elements are superimposed on the STEM images in Fig. 10. We found that the surface of the graphite particle after the long-term storage was generally covered with a thin layer of deposit, which will be consistent with that called SEI, reported in previous work. With respect to the chemical composition of SEI formed on graphite, inorganic and/or organic compounds containing F and P species are reported [3,7,8,18]. As shown in Fig. 10, F species as a main component of SEI are abundant both on the edge and on the basal planes of the graphite particles, even after the storage at 20 °C, which suggests

that the growth of SEI can proceed not only at the edge but also the basal planes of the graphite.

Different mechanisms have so far been presented for the SEI formation and growth at graphite electrodes [3,11,12,18]. Both chemical and electrochemical reduction processes can form inorganic and/or organic films at the surface of graphite particle. The reaction activity of the SEI formation might be dependent on the crystal plane, edge and basal planes, of the graphite particle. In Fig. 11, depth profiles of C, F and P elements are shown with the STEM images of the edge and basal planes of the graphite particles. From the observation for the edge part (A and B), there are no visible differences in the morphology and chemistry of SEI with the storage temperature. The thickness of SEI on the edge part of the sample stored at 60 °C was almost the same as that at 20 °C. On the other hand, the morphology and thickness of SEI depended much on the storage temperature at the basal plane (C and D). At lower temperature (20 °C), the average film thickness was 20–60 nm with formation of small semi-spherical deposits. The film thickness increased to about 100 nm after the electrode stored at 60 °C. These differences in the morphology and thickness of the film formed at the basal plane are probably reflected on the impedance profiles during the storage. As shown in Fig. 9, larger size of graphite tends to give higher rate of SEI growth, especially at high temperature. Higher rate of basal to edge planes in the larger size of graphite particle would be responsible for the larger changes in the interface resistance for storage at higher temperature. The possibility cannot be negligible that differences in the tap density among the particle size would influence the effective surface area inside the electrode.

The film formation process would also depend on other factors in the cell system, such as chemicals in electrodes and electrolytes. Influences of the electrolyte composition on the self-discharge behavior of synthetic graphite electrode are now under investigation, whose results will be reported in a separate paper.

4. Conclusion

Self-discharge characteristics of synthetic graphite electrodes with different particle sizes have been investigated by monitoring open-circuit potential (OCP), residual capacity, and ac impedance responses during and after the storage at different temperatures. The results are summarized as follows:

1. The OCP response reflected the extent of the self-discharge, or the changes in the stage structures of lithium graphite-intercalation compounds (Li-GICs) during the storage. Higher temperature and smaller particle size lead to higher rate of self-discharging.
2. The activation energy of the self-discharge process did not depend on the particle size of the graphite, but the specific surface area influenced the pre-exponential term, or frequency factor, in the Arrhenius equation. Thus, the particle size of graphite affects much the self-discharge rate, but does not influence the reaction mechanism.
3. Changes in the interface resistance obtained from the ac impedance response showed that the rate of SEI formation does not much depend on the particle size at lower temperature. However, higher rate of resistance increasing was observed for larger particle size electrode at higher temperature (60 °C).
4. STEM observation and EDX analysis of the surface proved that the SEI forms at both edge and basal planes of the lithiated graphite particle during and after the storage. The film formation at the basal plane was more influenced by the storage temperature, whose result might relate with differences in the impedance response during the storage among the samples with different particle sizes.

References

[1] B. Scrosati, J. Garche, J. Power Sources 195 (2010) 2419.
[2] J. Vetter, P. Novák, M.R. Wagner, C. Veit, K.-C. Möller, J.O. Besenhard, M. Winter, M. Wohlfahrt-Mehrens, C. Vogler, A. Hammouche, J. Power Sources 147 (2005) 269.
[3] R. Yazami, Electrochim. Acta 45 (1999) 87.
[4] R. Yazami, Y.F. Reynier, Electrochim. Acta 47 (2002) 1217.
[5] M. Holzapfel, F. Alloin, R. Yazami, Electrochim. Acta 49 (2004) 581.
[6] R. Yazami, M. Deschamps, S. Genies, J.C. Frison, J. Power Sources 68 (1997) 110.
[7] D. Aurbach, J.S. Gnanaraj, M.D. Levi, E.A. Levi, J.E. Fischer, A. Claye, J. Power Sources 97–98 (2001) 92.
[8] D. Aurbach, J. Power Sources 119–121 (2003) 497.
[9] E. Markevich, G. Salitra, M.D. Levi, D. Aurbach, J. Power Sources 146 (2005) 146.
[10] E. Markevich, E. Pollak, G. Salitra, D. Aurbach, J. Power Sources 174 (2007) 1263.
[11] S.E. Sloop, J.B. Kerr, K. Kinoshita, J. Power Sources 119–121 (2003) 330.
[12] L. Zhao, I. Watanabe, T. Doi, S. Okadam, J. Yamaki, J. Power Sources 161 (2006) 1275.
[13] T. Doi, L. Zhao, M. Zhou, S. Okada, J. Yamaki, J. Power Sources 185 (2008) 1380.
[14] R.P. Ramasamy, J.-W. Lee, B.N. Popov, J. Power Sources 166 (2007) 266.
[15] K. Ohue, T. Utsunomiya, O. hatozaki, N. Yoshimoto, M. Egashira, M. Morita, J. Power Sources 196 (2011) 3604.
[16] T. Utsunomiya, O. Hatozaki, N. Yoshimoto, M. Egashira, M. Morita, J. Power Sources, in press (2011), doi:10.1016/j.jpowsour.2011.05.066.
[17] C. Wang, X.-w. Zhang, A.J. Appleby, X. Chen, F.E. Litte, J. Power Sources 112 (2002) 98.
[18] D. Aurbach, M. Markovsky, K. Gamolsky, E. Levi, Y. Ein-Eli, Electrochim. Acta 45 (1999) 67.